Supporting Information

Highly Stable Artificial Synapse Consisting of Low Surface-Defect Van Der Waals and Self-Assembled Materials

Seyong Oh[†,§], *Sooyoung Jung*[†,§], *Muhammad Hasnain Ali*[†,§], *Jeong-Hoon Kim*[‖], *Hyeongjun Kim*[†], *and Jin-Hong Park*[*,†,‡]

[†] Department of Electrical and Computer Engineering and [‡] Sungkyunkwan Advanced Institute of Nano Technology (SAINT), Sungkyunkwan University, Suwon 16419, South Korea

[‖] Electrical and Computer Engineering Department University of California San Diego CA 92093, USA

Corresponding Author

*E-mail: jhpark9@skku.edu (J.-H. P)

Optical microscope image of *h*-BN/APTES/WSe_2 synaptic device

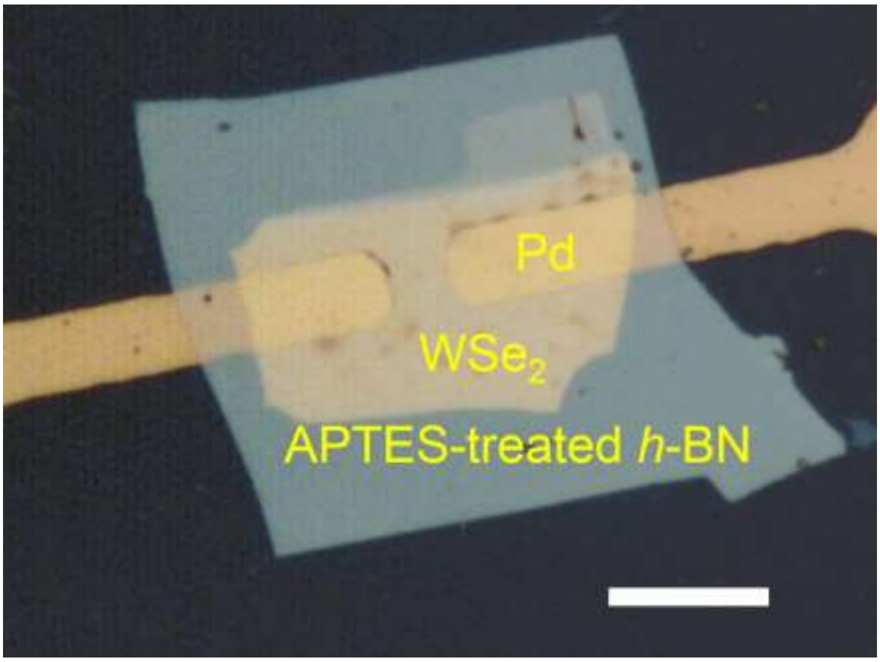

Figure S1. The channel length and width are 5 and 5 μm, respectively. The scale bar is 10 μm.

I_{post}–V_{WC} characteristic curves

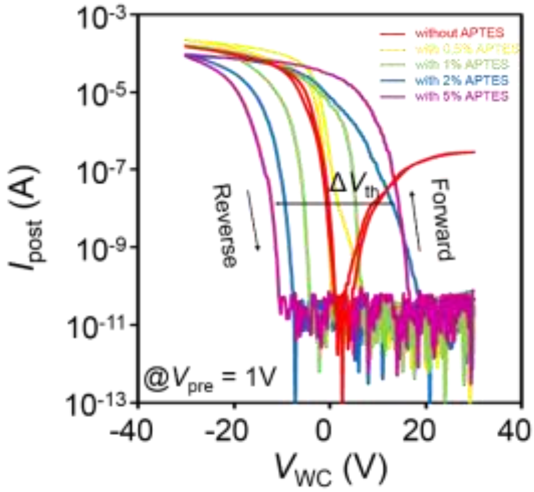

Figure S2. I_{post}–V_{WC} characteristic curves of synaptic devices with respect to various APTES concentrations (0.5%, 1%, 2%, and 5 %).

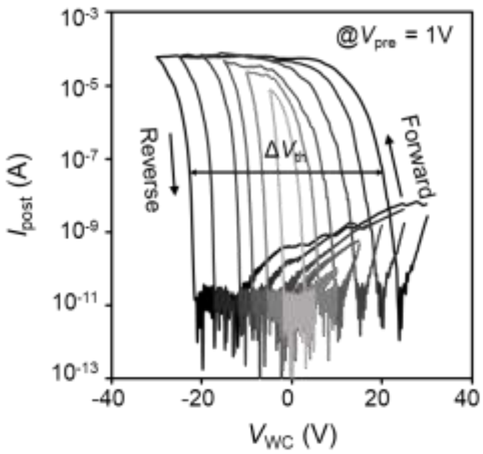

Figure S3. I_{post}–V_{WC} characteristic curves of synaptic devices with different weight control voltage (V_{WC}) values ranging from |5 V| to |25 V|."

Mechanism of long-term potentiation (LTP) and long-term depression (LTD) of *h*-BN/APTES/WSe_2 synaptic device

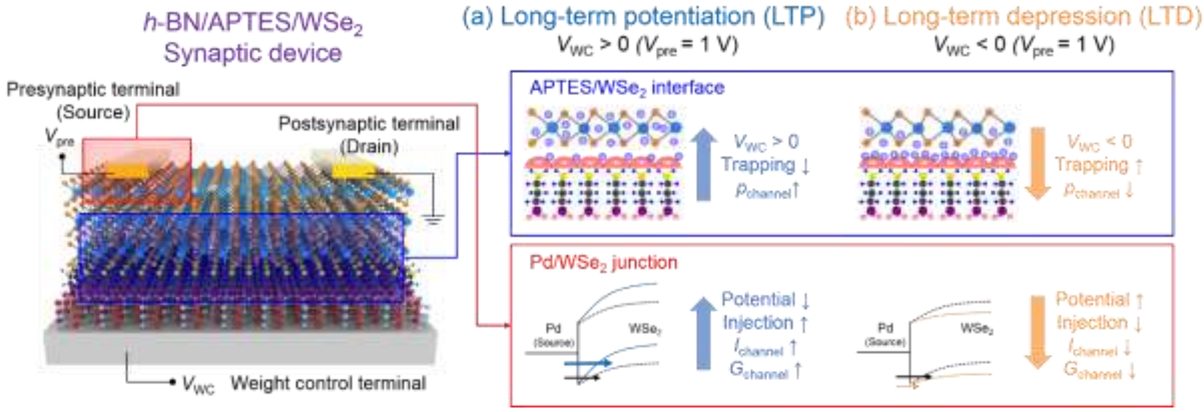

Figure S4. (a) When a positive V_{WC} is applied, some of the holes trapped at the APTES surface region are released (see APTES/WSe_2 interface), decreasing the WSe_2 channel potential (see Pd/WSe_2 junction). This moves up the WSe_2 energy band and consequently increases hole injection probability from the source electrode. As a result, the channel current increases, causing an increase in channel conductance ($G_{channel}$ ↑), which is called "long-term potentiation (LTP)". (b) On the other hand, when a negative V_{WC} is applied, hole carriers in channel region are trapped at the APTES surface, causing an increase in the WSe_2 channel potential. This drags down the WSe_2 energy band and thereby decreases the hole injection probability from the source electrode. Consequently, the channel current decreases, resulting in a decrease in channel conductance ($G_{channel}$ ↓), which is called, “long-term depression (LTD)”.

Nonlinearity analysis of the LTP/LTD characteristic curves

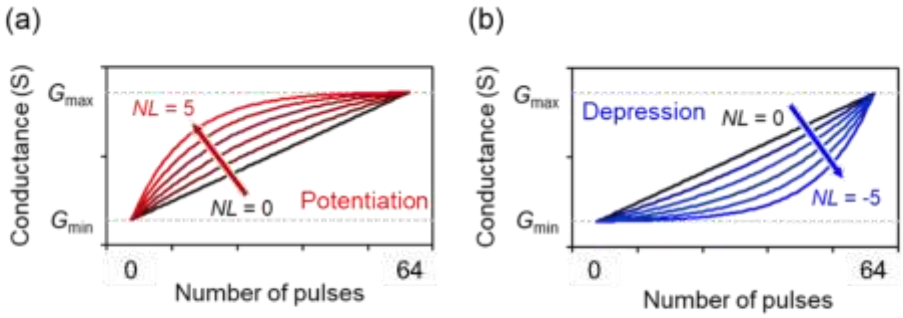

Figure S5. (a) Long-term potentiation (LTP) and (b) long-term depression (LTD) with respect to the nonlinearity (*NL*), ranging from 0 to 5.

Long-term potentiation (LTP) and long-term depression (LTD) characteristic curves measured at the pulse frequency of 100 Hz.

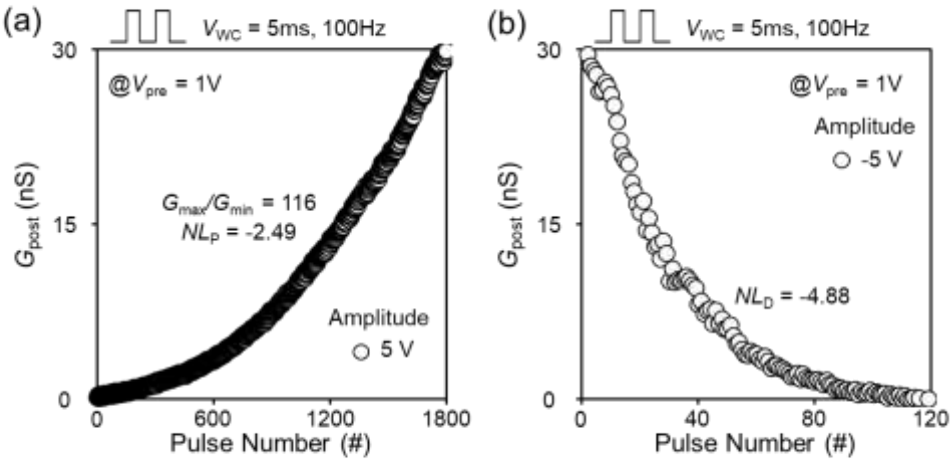

Figure S6. (a) LTP and (b) LTD characteristics with the pulse amplitudes of +5 V and −5 V, respectively. The pulse width and frequency were fixed at 5 ms and 100 Hz, respectively.

We investigated the LTP/LTD characteristics of the newly fabricated devices at a higher pulse frequency of 100 Hz. As shown in **Figures S6a** and **S6b**, our synaptic device responded well even at the pulse frequency of 100 Hz, where the read and write pulses were both of 5 ms. The dynamic range (G_{max}/G_{min}) was 116, and the nonlinearities for the LTP and LTD (NL_P and NL_D) were −2.49 and −4.88, respectively.

Van der Waals (vdW) synaptic device benchmarking

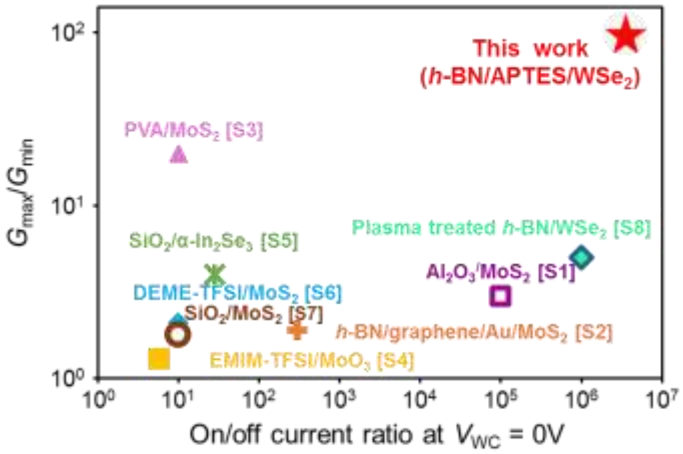

Figure S7. Benchmarking results against recently reported van der Waals synaptic devices in terms of the dynamic range (G_{max}/G_{min}) and on/off current ratio at V_{WC} = 0 V.

We compared our device with other van der Waals synaptic devices in terms of the dynamic range (G_{max}/G_{min}) and on/off current ratio at V_{WC} = 0 V (**Figure S7**). Our synaptic device exhibits relatively high G_{max}/G_{min} (>100) and on/off current ratio at V_{WC} = 0 V (>10^6).

SLP and MLP simulation results for the LTP/LTD response measured at the pulse frequency of 100 Hz

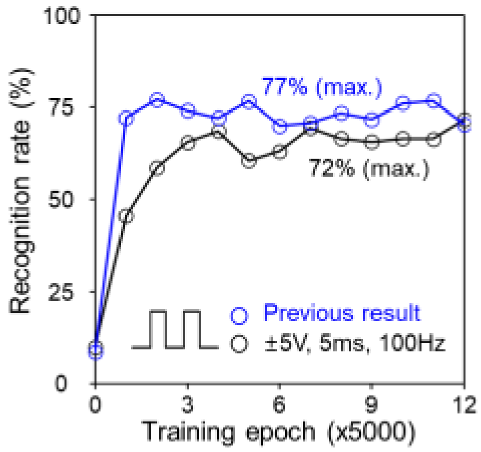

Figure S8. Recognition rate of single-layer perceptron (SLP)-based artificial neural network (ANN) as a function of training epochs for the high-frequency pulse condition (V_{WC} of 5 V, 5 ms, and 100 Hz).

Using the synaptic characteristic data obtained at a higher frequency (V_{WC} = ±5 V, 5 ms, and 100 Hz), we constructed a single-layer artificial neural network (ANN) of size 784 × 10 and conducted the training/recognition simulation for MNIST digit patterns. As shown in **Figure S8**, the recognition rate of the ANN was 72%, which was slightly lower than the previous result achieved at the low-frequency pulse condition (V_{WC} = ±5 V, 10 ms, and 16 Hz) but still acceptable.

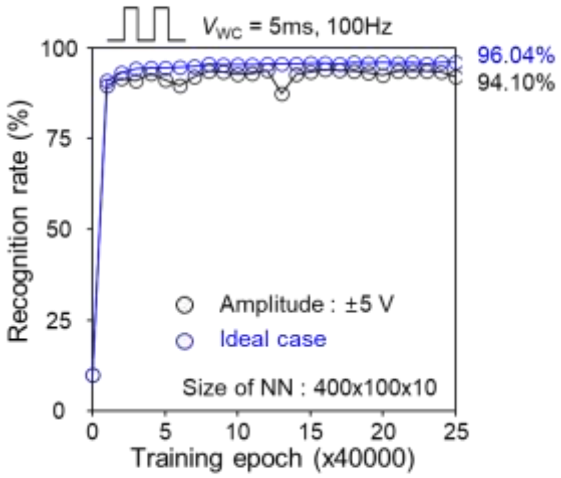

Figure S9. Recognition rate of the multi-layer perceptron (MLP)-based artificial neural network (ANN) as a function of training epochs (V_{WC} of 5 V, 5 ms, and 100 Hz).

To achieve a higher pattern recognition rate, we inserted a hidden layer into the single-layer neural network and thereby prepared a multi-layer perceptron (MLP)-based ANN of size 400 × 100 × 10. The simulation was conducted on the platform "MLP+NeuroSim ver. 1.0." Consequently, a higher recognition rate of 94.10% was achieved (**Figure S9**), which was close to the maximum recognition rate of the ideal case (96.04%).

Synaptic performance benchmarking

Device structure	*h*-BN/APTES/WSe_2 (This work)	Alkylated-GO/IGZO [S9]	CuPc/*p*-6P [S10]	Au/CNT [S11]	Cu^{2+}-doped salmon DNA [S12]	$MoSe_2$/$Bi2Se_3$/ PMMA [S12]
Type of update pulse	Electronic	Electronic	Optoelectronic	Electronic	Electronic	Optoelectronic
# of conductance states	64	100	85	120	64	11.3
Dynamic range	100	13.2	48.2	47	6.71	1.5
Nonlinearity	+3.13/–6.53	+5/–8	+1.38/–6.1	-	-20/18	-
Learning accuracy	78.3%	50% (voltage spikes only)	67%	70%	44%	70%

Table S1. Comparison table in terms of various synaptic performances such as the number of conductance states, dynamic range, nonlinearity, and learning accuracy (SLP-based ANN simulation only).

We summarized recent papers that studied synaptic performances in terms of the number of conductance states, dynamic range, nonlinearity, and learning accuracy (**Table S1**). Here, for an accurate comparison, we selected the papers in which the training/recognition simulation was conducted in a single-layer perceptron (SLP)-based artificial neural network (ANN). Our *h*-BN/APTES/WSe_2 hybrid synaptic device exhibited a relatively high dynamic range (~100) and moderate nonlinearities (+3.13/–6.53). Owing to such excellent synaptic characteristics, a relatively high recognition rate of 78.3% was achieved even with the SLP-based ANN.

Supporting Information Reference

[S1] Chen, H.; Liu, C.; Wu, Z.; He, Y.; Wang, Z.; Zhang, H.; Wan, Q.; Hu, W.; Zhang, D. W; Liu, M.; Liu, Q.; Zhou, P. Time-Tailoring van der Waals Heterostructures for Human Memory System Programming. *Adv. Sci*. **2019**, 6, 1901072.

[S2] Paul, T.; Ahmed, T.; Tiwari, K. K.; Thakur, C. S.; Ghosh, A. A High-Performance MoS_2 Synaptic Device with Floating Gate Engineering for Neuromorphic Computing. *2D Mater*. **2019**, 6, 045008.

[S3] Xie, D.; Jiang, J.; Hu, W.; He, Y.; Yang, J.; He, J.; Gao, Y.; Wan, Q. Coplanar Multigate MoS_2 Electric-Double-Layer Transistors for Neuromorphic Visual Recognition. *ACS Appl. Mater. Interfaces* **2018**, 10, 25943−25948.

[S4] Yang, C. S.; Shang, D. S.; Liu, N.; Shi, G.; Shen, X.; Yu, R. C.; Li, Y. Q.; Sun, Y. A Synaptic Transistor based on Quasi-2D Molybdenum Oxide. *Adv. Mater.* **2017**, 29 (27), 1700906.

[S5] Tang, B.; Hussain, S.; Xu, R.; Cheng, Z.; Liao, J.; Chen, Q. Novel Type of Synaptic Transistors Based on a Ferroelectric Semiconductor Channel. *ACS Appl. Mater. Interfaces* **2020**, 12, 24920−24928.

[S6] Du, J.-Y.; Ge, C.; Riahi, H.; Guo, E.-J.; He, M.; Wang, C.; Yang, G.-Z.; Jin, K.-J. Dual-Gated MoS_2 Transistors for Synaptic and Programmable Logic Functions. *Adv. Electron. Mater*. **2020**, 6, 1901408.

[S7] Han, K. H.; Kim, G.-S.; Park, J.; Kim, S.-G.; Park, J.-H.; Yu, H.-Y. Reduction of Threshold Voltage Hysteresis of MoS_2 Transistors with 3-Aminopropyltriethoxysilane Passivation and Its Application for Improved Synaptic Behavior. ACS Appl. Mater. Interfaces 2019, 11, 20949−20955.

[S8] Seo, S.; Jo, S.-H.; Kim, S.; Shim, J.; Oh, S.; Kim, J.-H.; Heo, K.; Choi, J.-W.; Choi, C.; Oh, S.; Kuzum, D.; Wong, H.-S. P.; Park, J.-H. Artificial Optic-Neural Synapse for Colored and Color-Mixed Pattern Recognition. *Nat. Commun.* **2018**, 9, 5106.

[S9] Sun, J.; Oh, S.; Choi, Y.; Seo, S.; Oh, M. J.; Lee, M.; Lee, W. B.; Yoo, P. J.; Cho, J. H.; Park, J.-H. Optoelectronic Synapse Based on IGZO-Alkylated Graphene Oxide Hybrid Structure. *Adv. Funct. Mater.* **2018**, 28, 1804397.

[S10] Qian, C.; Oh, S.; Choi,Y.; Kim, J.-H.; Sun, J.; Huang, H.; Yang, J.; Gao, Y.; Park, J.-H.; Cho, J. H. Solar-Stimulated Optoelectronic Synapse Based on Organic Heterojunction with Linearly Potentiated Synaptic Weight for Neuromorphic Computing. *Nano Energy*. **2019**, 66, 104095.

[S11] Kim, S.; Choi, B.; Lim, M.; Yoon, J.; Lee, J.; Kim, H.-D.; Choi, S.-J. Pattern Recognition

Using Carbon Nanotube Synapse Transistors with an Adjustable Weight Update Protocol. *ACS Nano* **2017**, 11, 2814−2822.

[S12] Kang, D.-H.; Kim, J.-H.; Oh, S.; Park, H.-Y.; Dugasani, S. R.; Kang, B.-S.; Choi, C.; Choi, R.; Lee, S.; Park, S. H.; Heo, K.; Park, J.-H. A Neuromorphic Device Implemented on a Salmon-DNA Electrolyte and its Application to Artificial Neural Networks. *Adv. Sci.* **2019**, 6, 1901265.

[S13] Wang, Y.; Yang, J.; Ye, W.; She, D.; Chen, J.; Lv, Z.; Roy, V. A. L.; Li, H. Zhou, K.; Yang, Q.; Zhou, Y.; Han, S.-T. Near-Infrared-Irradiation-Mediated Synaptic Behavior from Tunable Charge-Trapping Dynamics. *Adv. Electron. Mater.* **2020**, 6, 1900765.